

A massive black hole at the centre of the quiescent galaxy M32

Roeland P. van der Marel¹, P. Tim de Zeeuw², Hans–Walter Rix³ & Gerald D. Quinlan⁴

¹Institute for Advanced Study, Olden Lane, Princeton, New Jersey 08540, USA

²Sterrewacht Leiden, Postbus 9513, 2300 RA Leiden, The Netherlands

³Steward Observatory, University of Arizona, Tucson, Arizona 85721, USA

⁴Dept. of Physics and Astronomy, Rutgers University, PO Box 849, Piscataway, New Jersey 08855, USA

received 23 July 1996; accepted 10 January 1997; published 13 February 1997.

Massive black holes are thought to reside at the centres of many galaxies^{1,2}, where they power quasars and active galactic nuclei. But most galaxies are quiescent, indicating that any central massive black hole present will be starved of fuel and therefore detectable only through its gravitational influence on the motions of the surrounding stars. M32 is a nearby, quiescent elliptical galaxy in which the presence of a black hole has been suspected^{3–9}; however, the limited resolution of the observational data and the restricted classes of models used to interpret this data have made it difficult to rule out alternative explanations, such as models with an anisotropic stellar velocity distribution and no dark mass or models with a central concentration of dark objects (for example, stellar remnants or brown dwarfs). Here we present space-based high-resolution optical spectra of M32, which show that the stellar velocities near the centre of this galaxy exceed those inferred from previous ground-based observations. We use a range of general dynamical models to determine a central dark mass concentration of $(3.4 \pm 1.6) \times 10^6$ solar masses, contained within a region only 0.3 pc across. This leaves a massive black hole as the most plausible explanation of the data, thereby strengthening the view that such black holes exist even in quiescent galaxies.

We observed M32 with the Faint Object Spectrograph (FOS) on the Hubble Space Telescope (HST), on August 22, 1995. The COSTAR optics corrected the spherical aberration of the HST primary mirror. Spectra of the wavelength range 4572–6821 Å were taken through square apertures of 0.086'' and 0.215'', aligned on the nucleus and along the photometric major axis. The kinematical analysis was done by fitting each galaxy spectrum with the convolution of a template spectrum and a gaussian line-of-sight velocity profile. The details of the observations will be discussed by van der Marel, de Zeeuw & Rix (manuscript in preparation). The inferred kinematics are compared with the best ground-based data^{9,10} in Figure 1. The rotation curve derived from the HST spectra rises more steeply than that measured from the ground. The velocity dispersion from the HST aperture closest to the centre is $156 \pm 10 \text{ km s}^{-1}$. The average of the four independent dispersion measurements inside the central 0.1'' is 126 km s^{-1} , exceeding significantly the $85\text{--}95 \text{ km s}^{-1}$ measured from the ground.

Dynamical models are needed to infer the mass distribution from the kinematical data, and to test whether the observed velocities are consistent with a keplerian rise around a black hole. To this end we developed a new technique to construct fully general axisymmetric models that fit a given set of observations (Rix et al., van der Marel et al., Cretton et al., manuscripts in preparation). It is based on Schwarzschild's approach¹¹, and can be viewed as an axisymmetric generalization of the spherical technique of Richstone and collaborators^{5,6,12}. It consists of four steps: (i) an axisymmetric mass density is chosen that fits the M32 HST photometry¹³ after projection; (ii) the gravitational

potential is calculated, including a nuclear dark mass; (iii) a representative library of orbits is calculated; and (iv) a non-negative least-squares fit is performed to determine the combination of orbits that reproduces the assumed density and best fits the observational constraints.

Previous studies of M32 have used either axisymmetric models with distribution functions depending only on the two classical integrals of motion (the energy E and angular momentum L_z around the symmetry axis), $f(E, L_z)$, or spherical models with fully general distribution functions. Models of the first type take into account the flattening of M32 (projected axial ratio ~ 0.73), but have a special dynamical structure. They successfully fit the ground-based data when a nuclear dark mass is included^{7–9}, but they leave open the possibility that more general models might fit the data without a dark mass. Models of the second type allow for general anisotropy, but ignore the flattening of M32. These spherical models were used only to interpret some of the older M32 data⁵, and could not fit these without a nuclear dark mass⁶. However, we found that our less restricted axisymmetric models can easily fit these same data without a dark mass. So even though previous studies have shown that existing data are consistent with a nuclear dark mass in M32, it has not been shown that such a dark mass is required.

To improve this, we used our general axisymmetric technique to determine which models can fit both the new HST data and the most recent ground-based data^{9,10}. The models take the observational characteristics into account, and include velocity profile shape data (not available from the HST because of the limited spectral resolution of the FOS). Figure 2a shows a contour plot of the χ^2 of the fit for edge-on models with a dark central point mass. The free parameters are the V-band mass-to-light ratio Υ_V of the stellar population, and the dark mass M_\bullet . The models labelled A–D are the best-fitting models for four fixed values of M_\bullet . Figure 3 compares the predictions of these models with the observed major axis kinematics for each of the data sets. Models without a dark mass are ruled out; even the best-fitting model without a dark mass, Model A, fails to fit the nuclear HST velocity dispersions by $> 40 \text{ km s}^{-1}$. Model C has $M_\bullet = 3.4 \times 10^6 M_\odot$, and provides the overall lowest χ^2 . However, we would not necessarily expect our algorithm to constrain a single, best-fit choice of the potential, since a three-dimensional distribution function might have the freedom to adjust to changes of the potential without affecting the fit to the data. Numerical experiments showed that the structure in the χ^2 plot near the two minima could in fact be unreliable. We therefore do not claim that the local minimum labelled C is necessarily special, but conservatively estimate the allowed range for M_\bullet to be $(3.4 \pm 1.6) \times 10^6 M_\odot$. The uncertainty takes into account not only the observational errors in the data, but also the possible influence of small ($< 2 \text{ km s}^{-1}$ in the projected kinematics) numerical errors in the models (due to, for example, gridding and discretization). M32 need not be edge-on, but models constructed for inclination $i = 55^\circ$ gave similar results and the same allowed mass range. A full exploration of the range of possible inclinations is computationally prohibitive, but our results and previous work⁸ suggest that the inferred M_\bullet depends only weakly on the assumed inclination. Allowing for possible triaxiality is not likely to change these conclusions; they are due mostly to the radial behaviour of the potential, and not to its shape. The best-fitting models are not $f(E, L_z)$ models, but are similar in that they are tangentially anisotropic and require a similar dark mass.

To constrain the size of the dark mass, models were built with the point-mass potential replaced by a Plummer potential with the same mass, but with scale length ϵ . These were restricted to $f(E, L_z)$ models for simplicity; constraints on ϵ from the more general models should not differ by much. Figure 2b shows a contour plot of the χ^2 of the fit to the HST velocity dispersions, for edge-on models. The best fit has $\epsilon = 0$ (a point mass); models with $\epsilon \gtrsim 0.06''$ are ruled out.

The mass concentration thus has a half-mass radius $r_h = 1.30\epsilon \lesssim 0.08''$, implying a central density $\gtrsim 10^8 M_\odot \text{pc}^{-3}$ ($1'' = 3.39 \text{pc}$) and a mass-to-light ratio $\gtrsim 20$ inside $0.1''$. It cannot be a cluster of ordinary stars; that would evolve rapidly by stellar collisions¹³, and a change in mass-to-light ratio from ~ 2 at $1''$ to $\gtrsim 20$ at $0.1''$ would yield large broad-band colour gradients, ruled out by observations^{14,15}. It must be dark, either a massive black hole or a cluster of dark objects (e.g., stellar remnants, brown dwarfs, planets). No theory predicts the formation of such clusters—except perhaps^{16,17} for a cluster of small black holes of mass $m \simeq 5\text{--}10 M_\odot$, each—and most would not last for the age of the galaxy. A dark cluster is not an acceptable alternative to a massive black hole if it will collapse to a black hole in a short time, or expand or eject its mass through explosions or evolve in some other way that would make it observable (for then we would have to assume that it formed recently). Goodman and Lee¹⁸ considered possible dark clusters for M32, and argued that the clusters required $r_h \gtrsim 0.1''$ to be acceptable; these were consistent with ground-based data, which allowed⁶ ϵ to be as large as $0.4''$. We summarize and update the arguments here to show that all but the most implausible clusters are now ruled out.

A cluster of stellar remnants of mass $m \gtrsim 1 M_\odot$ would undergo core collapse in a short time, $5.5 \times 10^8 \text{yr} (M_\odot/m)(r_h/0.08'')^{3/2}$ for a Plummer model (and shorter for more concentrated models¹⁹). Neutron stars or small black holes would form binaries and merge during the collapse by dissipating energy through gravitational radiation²⁰. The binaries would not be able to stop the collapse until they had grown large through multiple mergers, and even then they would at most cause rapid oscillations in the central density, during which they would continue to grow¹⁷. One black hole would probably grow much faster than the others in a runaway manner²¹. Its mass would be modest at first, perhaps $10^3 M_\odot$, and might remain considerably smaller than $3 \times 10^6 M_\odot$. This model is not ruled out, but still requires a black hole (although embedded in a dark cluster) to fit the data. A cluster of white dwarfs would evolve similarly if the white dwarfs collapse to neutron stars upon merging; if they explode as supernovae instead the cluster would either lose mass or become observable.

A cluster of brown dwarfs or planets would have a long collapse time, but a short collision time¹⁸. The outcome of a collision depends on the ratio of the collision and binding energies²²: brown dwarfs of mass $m \gtrsim 0.05 M_\odot$ would merge with little mass loss, leading again to the growth of a massive object; planets or small brown dwarfs would disintegrate, leading to a massive gas cloud that would be unlikely to remain dark. The constraint that the collision time be longer than the age of the galaxy rules out clusters with $m \lesssim 0.03 M_\odot$. It might allow¹⁸ a cluster of brown dwarfs just below the hydrogen-burning limit ($m \simeq 0.08 M_\odot$) if $r_h \simeq 0.08''$, but another argument¹⁹ rules that out. The luminous stars of mass m_* that pass through the cluster would get trapped by dynamical friction in a time that depends only on the cluster density and not on m (if $m \ll m_*$), $5.5 \times 10^8 \text{yr} (M_\odot/m_*)(r_h/0.08'')^{3/2}$ (the collapse time given above reduced by m/m_*). The stars would sink to the centre, probably to merge into a massive object because binaries would be unable to eject stars from the deep potential well. A cluster with $r_h \simeq 0.08''$ would trap nearly 0.1% of the luminous stars, too many to be acceptable. This same argument limits the size of a bizarre dark cluster of elementary particles or tiny black holes to $r_h \lesssim 0.01''$.

The simplest and most plausible interpretation of the data is thus a single massive black hole. The X-ray emission from the centre of M32 could be from accretion onto the black hole, although its flux is low enough to be from a low-mass X-ray binary²³. The absence of a larger flux is explicable³: stars will be tidally disrupted¹⁸ only once every $10^3\text{--}10^4 \text{yr}$, and the luminosity from continuous gas accretion can be suppressed²⁴.

The arguments against a dark cluster in M32 rely mainly on the high density it would have ($\gtrsim 10^8 M_{\odot} \text{pc}^{-3}$). These arguments are weaker for the active galaxies M87 and NGC 4261, for which the dark matter density required by HST gas kinematics^{25,26} is only 10^5 (similar to the density of *luminous* material observed in some galactic nuclei and globular clusters). Stronger arguments can be made for three other black hole candidate galaxies requiring high densities: $10^{7.3}$ for the quiescent galaxy NGC 3115, as derived from HST stellar kinematics²⁷; $10^{9.8}$ for our own Galaxy, as derived from near-infrared velocity measurements of individual stars²⁸; and $10^{9.6-12.6}$ for the active galaxy NGC 4258, as derived from water maser observations^{29,30}. Together with our M32 results this provides compelling evidence for massive black holes in both active and quiescent galaxies.

Acknowledgements: We thank Nicolas Cretton, Lars Hernquist, Steinn Sigurdsson and Simon White for collaboration in various stages of this project. The results are based on observations with the NASA/ESA Hubble Space Telescope obtained at the Space Telescope Science Institute. STScI provided financial support through a GO grant and through a Hubble Fellowship awarded to RPvdM. STScI is operated under NASA contract by the Association of Universities for Research in Astronomy, Inc.

Correspondence should be addressed to R.P.v.d.M (email: marel@sns.ias.edu).

- [1]Rees, M. J. *Science* **247**, 817–823 (1990).
- [2]Haehnelt M. & Rees M. J. *Mon. Not. R. Astr. Soc* **263**, 168–178 (1993).
- [3]Kormendy, J. & Richstone, D. A. *Rev. Astr. Astrophys.* **33**, 581–624 (1995).
- [4]Tonry, J. L. *Astrophys. J.* **322**, 632–642 (1987).
- [5]Dressler, A. & Richstone, D. O. *Astrophys. J.* **324**, 701–713 (1988).
- [6]Richstone, D. O., Bower, G. & Dressler, A. *Astrophys. J.* **353**, 118–122 (1990).
- [7]Qian, E., de Zeeuw, P. T., van der Marel, R. P. & Hunter C. *Mon. Not. R. Astr. Soc* **274**, 602–622 (1995).
- [8]Dehnen, W. *Mon. Not. R. Astr. Soc* **274**, 919–932 (1995).
- [9]Bender, R., Kormendy, J. & Dehnen, W. *Astrophys. J.* **464**, L123–L126 (1996).
- [10]van der Marel, R. P. *et al. Mon. Not. R. Astr. Soc* **268**, 521–543 (1994).
- [11]Schwarzschild, M. *Astrophys. J.* **232**, 236–247 (1979).
- [12]Richstone, D. O. & Tremaine S. *Astrophys. J.* **296**, 370–378 (1985).
- [13]Lauer, T. R. *et al. Astr. J.* **104**, 552–562 (1992).
- [14]Lugger, P. M. *et al. Astr. J.* **104**, 83–91 (1992).
- [15]Crane, P. *et al. Astr. J.* **106**, 1371–1393 (1993).
- [16]Morris, M. *Astrophys. J.* **408**, 496–506 (1993).
- [17]Lee, H. M. *Mon. Not. R. Astr. Soc* **272**, 605–617 (1995).
- [18]Goodman, J. & Lee, H. M. *Astrophys. J.* **337**, 84–90 (1989).
- [19]Quinlan, G. D. *New Astron.* **1**, 255–270 (1996).
- [20]Quinlan, G. D. & Shapiro, S. L. *Astrophys. J.* **343**, 725–749 (1989).
- [21]Lee, H. M. *Astrophys. J.* **418**, 147–162 (1993).
- [22]Benz, W. & Hills, J. G. *Astrophys. J.* **323**, 614–628 (1987).
- [23]Eskridge, P. B., White III, R. E. & Davis, D. S. *Astrophys. J.* **463**, L59–L62 (1996).

- [24] Narayan, R., Yi, I., Mahadevan, R. *Nature* **374**, 623–625 (1995).
- [25] Harms, R. J. *et al. Astrophys. J.* **435**, L35–L38 (1994).
- [26] Ferrarese, L., Ford, H. C. & Jaffe, W. *Astrophys. J.* **470**, 444–459 (1996).
- [27] Kormendy, J. *et al. Astrophys. J.* **459**, L57–L60 (1996).
- [28] Eckart, A. & Genzel, R. *Nature* **383**, 415–417 (1996).
- [29] Miyoshi, M. *et al. Nature* **373**, 127–129 (1995).
- [30] Maoz, E. *Astrophys. J.* **447**, L91–L94 (1995).

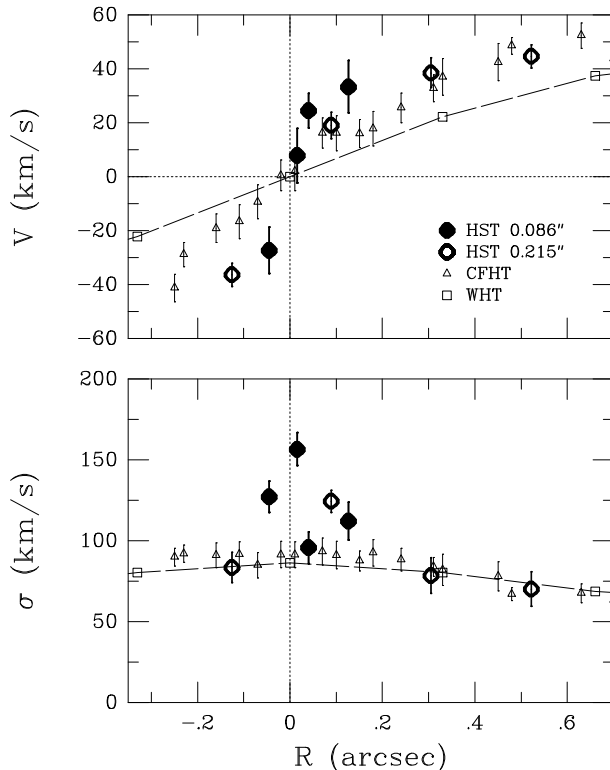


Fig. 1.— Stellar rotation velocities V (top panel) and velocity dispersions σ (bottom panel) in M32, as function of major axis distance. The new HST data (aperture sizes indicated in the figure) are compared with ground-based data obtained at the William Herschel Telescope¹⁰ (WHT; resolution $\sim 0.8''$; connected by a line for illustration; error bars smaller than plot symbols) and the Canada-France Hawaii Telescope⁹ (CFHT; resolution $\sim 0.5''$). The HST data were obtained with the G570H grating on the FOS red detector, and were calibrated using arc lamp spectra obtained during Earth occultations. The pointing accuracy was limited by target acquisition uncertainties ($\sim 0.02''$) and thermal effects on the spacecraft and Fine Guidance Sensors (increasing to $\sim 0.1''$ during the 14 hours of the observations). The actual aperture position for each observation was calculated *post hoc* to $\sim 0.01''$ accuracy from models based on HST photometry¹³ for the target acquisition data, the observed count rate in each spectrum, and a verification image obtained at the end of the observations. The template spectrum used for the kinematical analysis was a mix of ground-based spectra of stars of different spectral types, chosen to best match the M32 spectrum. The kinematical results were corrected for line-spread-function differences between the galaxy and template spectra. The line spread function for each galaxy spectrum was calculated from models for the distribution of the galaxy light within the aperture, taking into account the grating broadening function and the finite size of the detector diodes. The relatively low velocity dispersion inferred for the HST aperture second-closest to the nucleus might have been affected by a systematic error, but none could be identified.

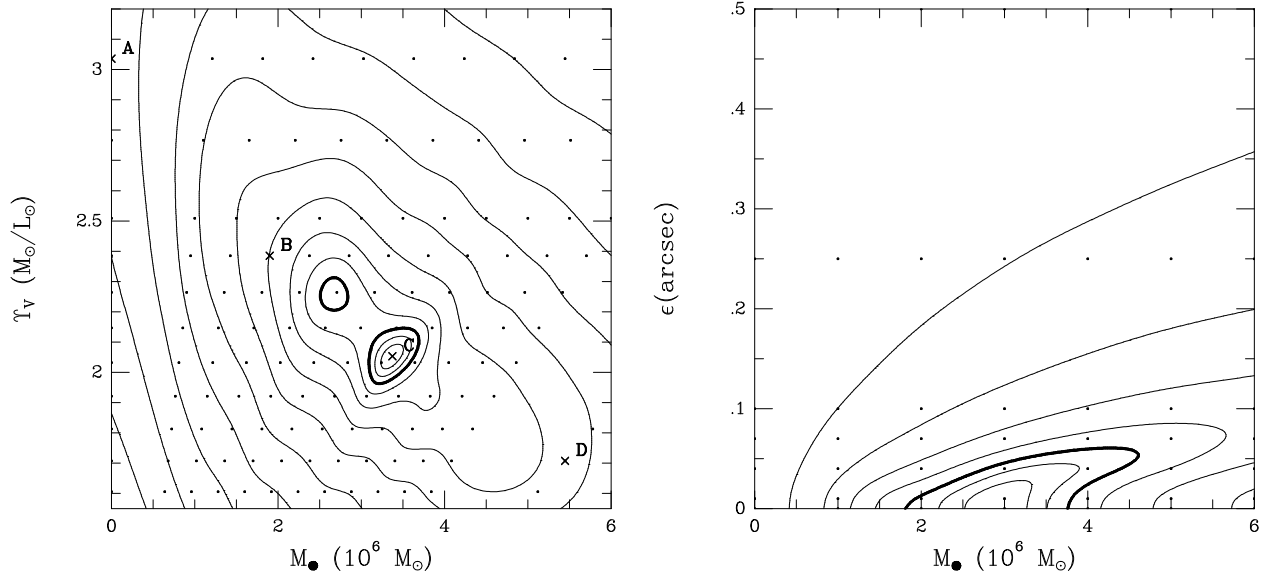


Fig. 2.— *a*, Contours of the χ^2 that measures the quality of the fit to the combined HST and ground-based kinematical M32 data, for edge-on models with a fully general dynamical structure. The model parameters M_\bullet and Υ_V are the dark nuclear point mass and the V-band stellar mass-to-light ratio. The dots indicate models that were calculated. The predictions of the models labelled A–D are shown in Fig. 3. The contours were obtained through spline interpolation. The first three contours define the formal 68.3%, 95.4% and (heavy contours) 99.73% confidence regions. Subsequent contours are characterized by a factor two increase in $\Delta\chi^2 = \chi^2 - \chi_{\min}^2$. The confidence values assume that there are only gaussian random errors in the data, and no numerical errors in the models. In reality there are numerical errors in the models, but they are known to be small (see the legend of Figure 3). Tests show that these errors can be responsible for the presence of the second (local) minimum in the χ^2 contours (although this might also be real), but that they cannot make the predictions of models with $M_\bullet < 1.8 \times 10^6 M_\odot$ or $M_\bullet > 5.0 \times 10^6 M_\odot$ consistent with the data at the formal 99.73% confidence level. We therefore conclude that $M_\bullet = (3.4 \pm 1.6) \times 10^6 M_\odot$. *b*, Contours of the χ^2 that measures the quality of the fit to the HST velocity dispersions, for edge-on $f(E, L_z)$ models with an extended dark nuclear object with scale length ϵ (and with $\Upsilon_V = 2.51$ to best fit the data outside the central arcsec for this assumed dynamical structure). A point mass ($\epsilon = 0$) provides the best fit; models with $\epsilon \gtrsim 0.06''$ are ruled out.

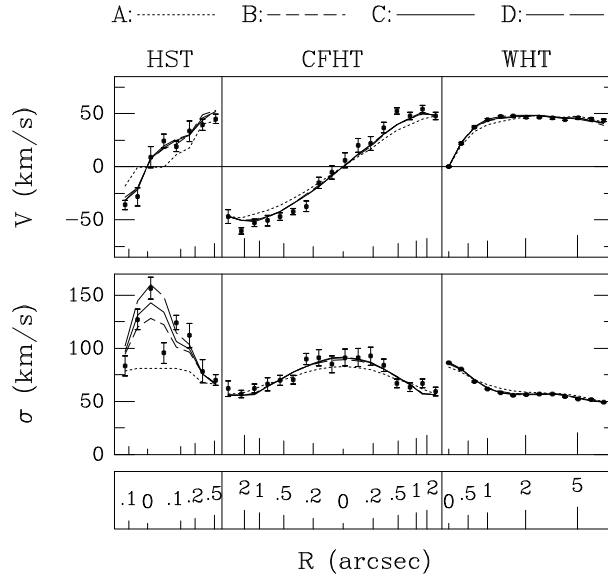


Fig. 3.— Predicted rotation velocities V and velocity dispersions σ of models A–D in Figure 2, compared with the major axis data from the HST, CFHT and WHT. Data points are plotted equidistantly along the abscissa. Corresponding major axis distances are given in the bottom panel. The WHT measurements are averages of data obtained at positive and negative radii. The displayed quantities form only a subset of all the data that were fitted (for the ground-based observations^{9,10}, velocity profile shape data and position angles other than the major axis are also available). Model C is the edge-on model with the lowest χ^2 , and has a dark nuclear point mass $M_{\bullet} = 3.4 \times 10^6 M_{\odot}$. Models B and D are (approximately) the best-fitting models for $M_{\bullet} = 1.9$ and $5.4 \times 10^6 M_{\odot}$, respectively. Model A is the best fit without a dark mass. This model is ruled out. It is already marginally ruled out by the ground-based CFHT and WHT data, but only the HST velocity dispersion measurements make the case clear-cut. The accuracy of the model predictions was assessed by having them reproduce the known results for $f(E, L_z)$ models^{7,8}. From these tests we conclude that numerical errors in our models are sufficiently small not to be of influence to the conclusions of our paper (they are $< 2 \text{ km s}^{-1}$ in the projected kinematics and < 0.01 in the Gauss-Hermite moments¹⁰ of the velocity profiles).